Available online at www.sciencedirect.com
ScienceDirect
International Journal of Heat and Mass Transfer 50 (2007) 15–25
International Journal of HEAT and MASS TRANSFER
www.elsevier.com/locate/ijhmt

Effect of rotation on leading edge region film cooling of a gas turbine blade with three rows of film cooling holes

Jaeyong Ahn [a], M.T. Schobeiri [a], Je-Chin Han [a,*], Hee-Koo Moon [b]

[a] Department of Mechanical Engineering, Texas A&M University, College Station, TX 77843-3123, United States
[b] Solar Turbines Incorporated, 2200 Pacific Highway, San Diego, CA 92101, United States

Received 4 November 2005; received in revised form 30 June 2006
Available online 6 September 2006

Abstract

Effect of rotation on detailed film cooling effectiveness distributions in the leading edge region of a gas turbine blade with three showerhead rows of radial-angle holes were measured using the Pressure Sensitive Paint (PSP) technique. Tests were conducted on the first-stage rotor blade of a three-stage axial turbine at three rotational speeds. The effect of the blowing ratio was also studied. The Reynolds number based on the axial chord length and the exit velocity was 200,000 and the total to exit pressure ratio was 1.12 for the first-stage rotor blade. The corresponding rotor blade inlet and exit Mach number was 0.1 and 0.3, respectively. The film cooling effectiveness distributions were presented along with the discussions on the influences of rotational speed, blowing ratio, and vortices around the leading edge region. Results showed that different rotation speeds significantly change the film cooling traces with the average film cooling effectiveness in the leading edge region increasing with blowing ratio.

Keywords: Gas turbine; Film cooling; Rotating blade; Leading edge; Pressure sensitive paint (PSP)

1. Introduction

The turbine inlet temperature of modern gas turbine engines has been increased to achieve higher thermal efficiency. However, the increased inlet temperature can result in material failure of the turbine system due to the higher heat transfer and induced thermal stresses. In order to overcome the potential problem from the high temperature environment and prevent failure of turbine components, film cooling has been widely employed as an active cooling method. In a film cooled component, relatively cooler air is injected through several discrete holes which forms a protective film between the hot mainstream gas and the turbine component to maintain the surface at a lower temperature, thus protecting the turbine component from failure. However, excessive use of coolant can reduce the gain of the higher inlet temperature because the consumption of compressed air and the mixing losses between the hot mainstream flow and coolant reduce the thermal efficiency of entire system. Thus, many investigations have been conducted to understand the physical phenomena regarding the film cooling process and to find better film-hole configurations that can provide better protection with less amount of coolant. A comprehensive compilation of the available internal and external turbine cooling techniques used in the gas turbine industry has been published by Han et al. [1] in their book.

Many studies on the film cooling have been performed on the blade in a cascade. Nirmalan and Hylton [2] investigated the effects of various flow and temperature parameters on film cooling in a turbine vane cascade whose conditions were similar to the ranges of actual engines. Abuaf et al. [3] presented heat transfer coefficients and film effectiveness for a film cooled vane. The heat transfer coefficient on the pressure surface showed very little effect of film injection while the suction side heat transfer coefficient showed a significant

* Corresponding author.
E-mail address: jc-han@tamu.edu (J.-C. Han).

0017-9310/$ - see front matter © 2006 Elsevier Ltd. All rights reserved.
doi:10.1016/j.ijheatmasstransfer.2006.06.028

Nomenclature

C	oxygen concentration
d	diameter of film cooling holes (1.19 mm)
I	pixel intensity for an image
M	average blowing ratio ($=\rho_c V_c/\rho_m V_m$)
P_{O_2}	partial pressure of oxygen
P	static pressure
p	span-wise distance between film cooling holes
PS	blade pressure side
r^*	immersion ratio, $(r - r_{hub})/(r_{tip} - r_{hub})$
SS	blade suction side
x	stream-wise distance from leading edge stagnation line
η	local film cooling effectiveness

Subscripts

c	coolant
m	mainstream
air	mainstream air with air as coolant
mix	mainstream air with nitrogen as coolant
ref	reference image with no mainstream and coolant flow
blk	image without illumination (black)

increase. Cruse et al. [4] studied the effect of leading edge shapes. They measured the film cooling effectiveness using an infrared camera with circular and elliptic leading edge geometries. They observed very similar results for both leading edge geometries. Ekkad et al. [5] studied the combined effects of unsteady wake and free stream turbulence on the film cooling effectiveness and the heat transfer coefficient with air and CO_2 film injection, respectively. They found higher heat transfer coefficients and lower film cooling effectiveness compared to the individual effects. Cutbirth and Bogard [6] studied the effects of coolant-to-mainstream density ratio on film cooling effectiveness on a simulated turbine vane model using an infrared camera technique.

More detailed investigations were performed on the leading edge region because it has the highest heat transfer level due to flow stagnation and affects the heat transfer and aerodynamics over the entire blade. Luckey et al. [7] simulated the airfoil leading edge using a cylinder with several film cooling rows. The holes were located at angles of 20°, 30°, and 40° to the surface in the span-wise direction. The coolant to mainstream density ratio was 2.15, which is a typical engine condition. They correlated their result for the optimum blowing ratio in terms of coolant to mainstream velocity ratio and injection angle. Mick and Mayle [8] studied the effect of coolant blowing ratio and film cooling-hole location on the stagnation region of a semicircular leading edge with a flat body. They presented heat transfer coefficient and film effectiveness results for two rows of holes at ±15° and ±44° from stagnation with the coolant blowing ratio from $M = 0.38$ to 0.97. Karni and Goldstein [9] studied the effect of blowing ratio and injection location on the mass transfer coefficient using a cylindrical leading edge model. Mehendale et al. [10] and Mehendale and Han [11] investigated the effect of free stream turbulence on heat transfer and film cooling effectiveness using a cylindrical leading edge model. They showed that the coolant jets are maintained over a longer distance at lower free stream turbulence. Ou et al. [12] presented the effect of film-hole location and inclined film slots on the leading edge film cooling heat transfer using a cylindrical leading edge model. They showed that two-row injection performs better at a lower blowing ratio while, at higher blowing ratio, two-row injection and one-row injection film effectiveness distributions overlap. Mehendale and Han [13] studied the Reynolds number effect on leading edge film effectiveness and heat transfer coefficients. Their result showed that an increase in Reynolds number increases both the heat transfer coefficients and film cooling effectiveness because the momentum of the flow near the wall is higher and causes more deflection of film cooling jet. Salcudean et al. [14] investigated the effect of coolant to mainstream density ratio using air and CO_2 as coolant gases. They used the heat/mass transfer analogy to measure adiabatic wall effectiveness. Funazaki et al. [15] studied the effect of unsteady wake on the leading edge film cooling effectiveness. They used a spoked-wheel-type generator to simulate the periodic unsteady wake effect on turbine blade film cooling. They pointed out that the effect of length scale should be considered, and the presence of unsteady wakes may reduce film cooling effectiveness. Ekkad et al. [16] presented the effect of coolant density and free-stream turbulence on a cylindrical leading edge model using a transient liquid crystal technique to obtain the detailed heat transfer coefficient and film effectiveness distributions. They also used CO_2 and air as coolant gases to simulate the density ratio effect. They determined that the film cooling effectiveness values for air as the coolant are highest at lower blowing ratios and decrease with an increase in blowing ratio. However, with CO_2 as the coolant, highest film cooling effectiveness is obtained at a blowing ratio of 0.8. Ou and Rivir [17] examined the effect of turbulence intensity, blowing ratio, and Reynolds number using a transient liquid crystal image method on a large scale symmetric circular leading edge. Their result showed similar trends with previous research and confirmed the heat flux reduction due to the film cooling. Much research was also conducted on the effect of film-hole geometry. Reiss and Bölcs [18] and Kim and Kim [19] studied the effect of injection hole

shape using a cylinder model and showed that holes with a laid back type widened exits provided higher film cooling effectiveness compared to the standard cylindrical holes.

Despite the numerous studies on the film cooling effectiveness, most of them were simulated in a cascade blade or in a wind tunnel using a flat plate or a cylindrical model. Only a few results about film cooling effectiveness under turbine rotating conditions are available in open literature due to the difficulty in conducting this type of experiments. Dring et al. [20] investigated film cooling performance in a low speed rotating facility. A film cooling hole was located on both the pressure and suction sides. They used ammonia and Ozalid paper to qualitatively observe the coolant trace while the quantitative tests were conducted using thermocouples. Their results show that the film coolant had only a small radial displacement, similar to flat plate results, on the suction side. On the pressure side, the film coolant trace had a large radial displacement toward the blade tip due to rotation. Takeishi et al. [21] also reported the film cooling effectiveness distributions on a low speed stator–rotor stage using a rotating rig with a one-stage turbine model. They simulated actual flow velocity triangles and pressure ratios of an actual heavy-duty gas turbine. The blowing ratios were similar to engine conditions ($M = 0.6$–1.0) while the coolant to mainstream density ratio was unity, whereas the coolant density ratio is 1.5–2.5 in real engine conditions. They sampled the gas along the blade surface at several locations and analyzed them using gas chromatography. They also simulated similar flow conditions in a cascade blade and compared with the data from the rotating blade. The results showed that the results from the cascade blade and the rotating blade matched well on the suction side while the rotating blade film cooling results decreased more rapidly than the cascade blade results on the pressure side. They explained that this phenomenon is due to the radial flow and strong mixing on the pressure side due to rotation. They also noted that the overall film effectiveness value on the suction side is higher than that of pressure side, and that strong lateral mixing cause fundamentally different role of concave (pressure side) and convex (suction side) surfaces on boundary layer stability. Abhari and Epstein [22] investigated time-resolved measurements of heat transfer on a fully cooled transonic turbine stage. Using a short-duration blow down turbine test facility, they simulated full engine parameters. The coolant was supplied through the film cooling holes on the pressure and the suction sides, but no film cooling holes were located on the leading edge region. They distributed a number of thin-film heat flux gages along the blade surface to measure the time-resolved heat flux distributions. Their results showed that the film cooling has very little effect on the pressure side heat transfer level, while a strong effect of film cooling is observed on the entire suction side surface.

In this study, pressure sensitive paint (PSP) technique was used to measure the detailed film cooling effectiveness distributions in the leading edge region of a rotating turbine blade. Note that PSP technique is based on the mass transfer analogy. Thus, it is free from the heat conduction effects, which cannot be avoided in the standard heat transfer measurement methods. This technique was proposed by Zhang et al. [23]. In their study, the film cooling effectiveness distributions were measured on the flat plate using PSP technique, and the results were validated by the gas chromatography measurements. They also applied PSP technique to measure the film effectiveness distributions on the turbine nozzle end-wall region [24,25]. Ahn et al. [26] and Mhetras et al. [27] used similar PSP technique to measure the film cooling effectiveness distributions on the cascade blade tip region, and on the squealer rim wall region, respectively. Wright et al. [28] conducted an assessment of steady state PSP, TSP (temperature sensitive paint), and IR (infrared) measurement techniques for flat plate film cooling. Gao et al. [29] compared the steady state PSP and transient IR measurement techniques for the non-rotating leading edge region film cooling.

This study is aimed to investigate the effects of the rotational speed and blowing ratio on the leading edge region film cooling effectiveness of a rotating turbine blade with three rows of radial-angle holes. Another objective of this study is applying PSP technique on a rotating blade in order to determine heat-conduction-free detailed film cooling effectiveness distributions. The rotational speed was maintained to be 2400, 2550, and 3000 rpm and the averaged blowing ratio was controlled to be 0.5, 1.0, and 2.0, respectively. The experimental results of the detailed film cooling effectiveness distribution on the leading edge region of a rotating turbine blade will be helpful in understanding the physical phenomena regarding the leading edge film cooling and useful in designing more efficient cooled-turbine rotor blades.

2. Experimental setup

2.1. Research type turbine facility

To address the major turbine efficiency, performance, heat transfer and flow research issues, Schobeiri and his co-workers [30,31] designed a state-of-the-art multipurpose turbine research facility with a versatile research turbine as its core component. The modular structured design of the research turbine enables incorporation of up to four turbine stages. The stator and rotor blades may be of any arbitrary design, ranging from zero degree of reaction cylindrical blades to higher reaction 3-D blades. Test blades of high, intermediate, or low pressure turbine units may be used. The facility is capable of accurately measuring the efficiency and performance of the entire turbine engine. In particular, the sophisticated inter-stage traversing system provides detailed flow and temperature profiles between the turbine stages.

The overall layout of the test facility is shown in Fig. 1. It consists of a 300HP electric motor connected to a frequency controller which drives the compressor component. A three-stage centrifugal compressor supplies air with a

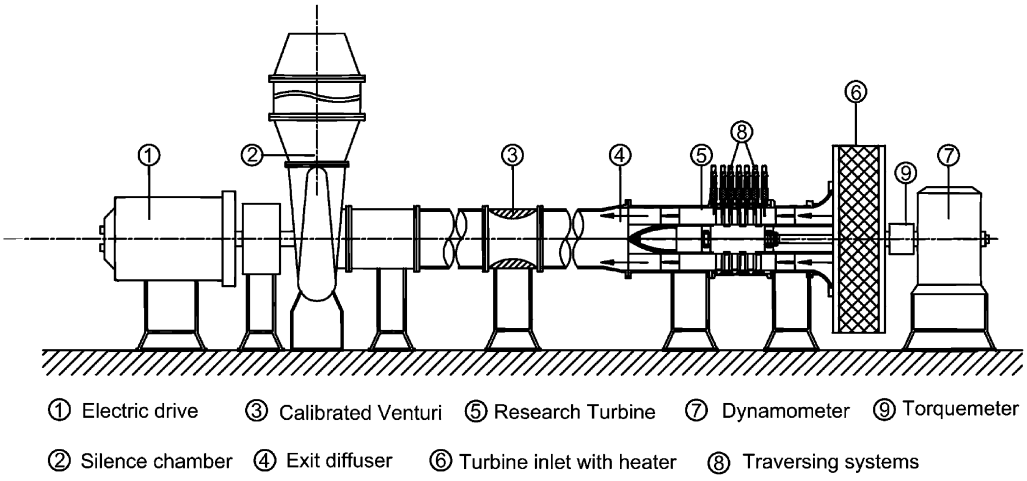

Fig. 1. Overall layout of TPFL-research turbine facility, from Schobeiri et al. [30].

maximum pressure difference of 55 kPa and a volume flow rate of 4 m^3/s. The compressor operates in suction mode and the pressure and volume flow can be varied by a frequency controller from 0 to 66 Hz. A pipe fitted with a transition piece connects the compressor to a Venturi mass flow meter which is used to measure the mass flow through the turbine component. An exit diffuser serves as a smooth transition piece between the turbine component and the Venturi. The three-stage turbine with a fully automated data acquisition system is the core component of the test facility. The turbine inlet has an integrated heater that prevents condensation of water from humid air expanding through the turbine during the test. The turbine shaft is connected through a flexible coupling with one end of a high precision torque meter that has a maximum rotational speed of 8500 rpm and a maximum torque of 677.9 N m. The accuracy of this torque meter is ±0.02% of full scale. The other end of the torque meter is coupled via a second flexible coupling with an eddy current low inertia dynamometer with the maximum power of 150 kW, a maximum torque of 500 N m, a maximum rotational speed of 8000 rpm, a torque accuracy of ±1.25 N m (a minimum requirement: 0.25% of a full scale load), and a rotational speed accuracy of ±1 rpm. The dynamometer is controlled by a Texcel V4-EC controller acquisition computer. The major components of this facility were chosen such that the engine efficiency accuracy requirements of less than 0.5% are satisfied. Fig. 2 shows a three-stage air turbine component with its dimensions and operating conditions specified in Table 1. For the current investigations, fully cylindrical 2-D blades are used. A conceptual view of each stage is shown in Fig. 3. The blades are mounted on the rotor cylinder, which is connected to the shaft via two locking mechanisms. Detailed flow characteristics of this turbine can be found in the study of Schobeiri et al. [30,31]. They used a 5-hole probe to provide flow angles, loss characteristics, pressure contours at several sections, and other aerodynamic performance at design point and off-design conditions.

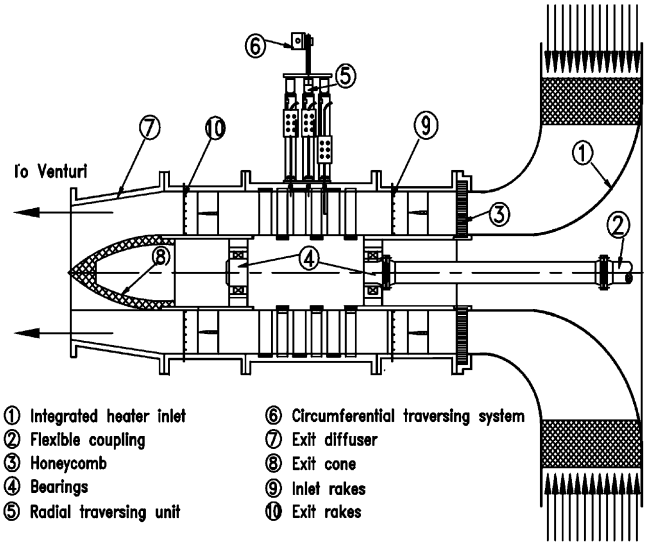

Fig. 2. Three-stage research turbine components, from Schobeiri et al. [30].

2.2. Modification on the turbine

For film cooling and heat transfer investigations, a module has been added to the system to enable precise measure-

Table 1
Turbine dimensions and operating conditions

Item	Specification	Item	Specification
Stage no.	$N = 3$	Mass flow	ms = 3.728 kg/s
Tip diameter	$D_t = 685.8$ mm	Speed range	$n = 1800$–3000 rpm
Hub diameter	$D_h = 558.8$ mm	Design speed	$n_D = 2550$ rpm
Blade height	$Bh = 63.5$ mm	Current speed	$n = 2400$–3000 rpm
Blade no.	Stator 1 = 58	Inlet pressure	$p_{in} = 101.356$ kPa
Blade no.	Rotor 1 = 46	Exit pressure	$p_{ex} = 71.708$ kPa
Blade no.	Stator 2 = 52	Blade no.	Stator 3 = 56
Blade no.	Rotor 2 = 40	Blade no.	Rotor 3 = 44
Power		$P = 80.0$–110.0 kW	

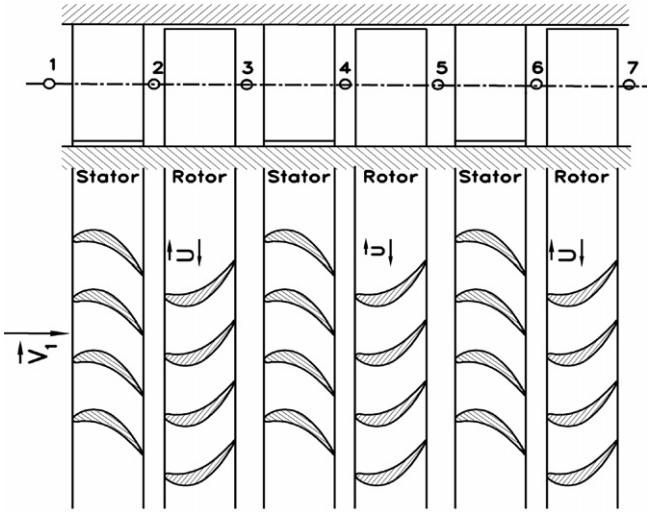

Fig. 3. Conceptual view of three-stage turbine, from Schobeiri et al. [31].

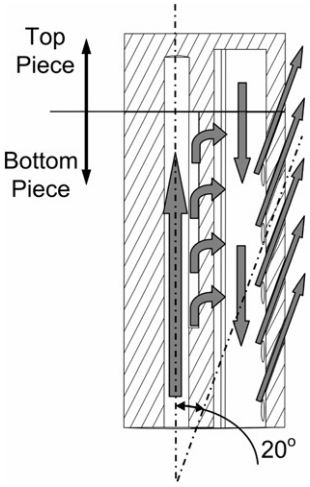

Fig. 5. Coolant path inside the blade.

ment of film cooling effectiveness on rotating blades using PSP measurement techniques. To supply coolant to the blade, the rotor cylinder and turbine shafts were modified as shown in Fig. 4. A rotary seal was adapted to prevent any leakage between rotating and non-rotating components. The coolant gas is supplied through the hollow shaft and fills inside of the rotor cylinder. Then the coolant is injected into the blades through the hollow bolts.

Fig. 5 shows the coolant path inside the blade at the first rotor stage. The blade consists of top and bottom pieces due to the manufacturing constraints and its total height and axial chord length are 63.5 mm and 38.1 mm, respectively. The coolant is injected into the leading edge plenum connected to a radial slot. This design was applied to ensure a uniform coolant discharge from the plenum to the film cooling holes. Then, the coolant gas is finally injected into the mainstream through the discrete showerhead hole array on the leading edge.

There are 15 film cooling holes in three rows; pressure side, suction side, and center row (Fig. 6). Each row has

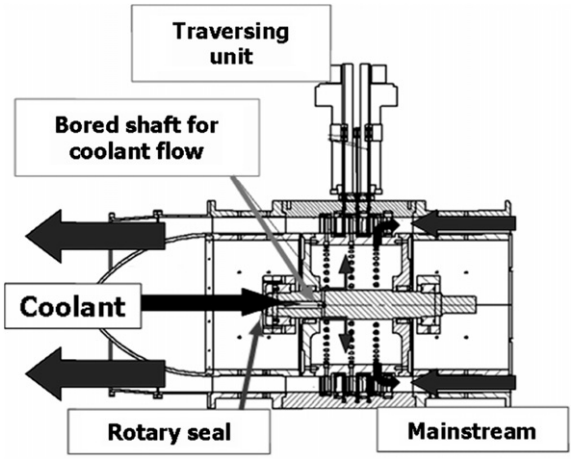

Fig. 4. Flow path of the coolant gas.

Fig. 6. Modified film cooling blade with three rows of radial-angle holes.

five film cooling holes and those in the center row are staggered to the holes of the pressure and suction side row. The distance between the film cooling holes (p) is 9.5 mm in the span-wise direction and the film hole diameter (d) is 1.19 mm ($p/d = 5.97$). The pressure and suction side rows are respectively located at 23.58 from the leading edge stagnation line in stream-wise direction. The film cooling holes were oriented to the span-wise radial direction and inclined to the surface by 20°. In order to prevent any imbalance, the modified blades were diametrically mounted.

2.3. Optical components setup

Fig. 7 depicts the schematic drawing of the optical components used for data acquisition. A 6 W Argon ion laser, whose wavelength was 488 nm, illuminated the PSP coated blade. A borescope was used to enable optical access to the

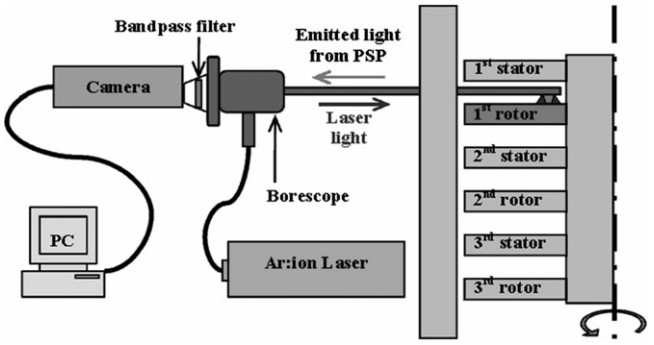

Fig. 7. Schematic drawing of the optical components.

blade leading edge region. It was inserted between the trailing edge of 1st stator and the leading edge of the 1st rotor and was confirmed to be rigid under load. It had a 90° direction of view and a ±45° field of view and its diameter was 5.77 mm. Both the exciting light from the laser and the emitted light from the PSP coating were delivered through the bore scope using separate paths of fiber optic cables embedded in the bore scope. A 12-bit scientific grade CCD camera (High speed Sensicam with CCD temperature maintained at −15 °C using two-stage peltier cooler) with an exposure time of 15 μs was employed to measure the emitting light intensity. At the given optical setup and exposure time, the averaged number of photons detected by a pixel is about 1500 while the full-well capacity of the camera is 35,000 e^-. After averaging 200 images, it gives 0.2–0.4% shot noise error for the given pressure range. The camera was triggered by a signal from an angular position sensor attached on the shaft. By detecting the same angular position, the images from the camera had the same view angle and were able to be averaged without blurring the information. In addition, an optical 600 nm long pass filter was placed between the camera and the borescope to block any reflected light and to record only the emitted light from the PSP. Spectral characteristics of the current PSP were also considered to choose the wavelengths for excitation (blue at 488 nm) and return (orange) signals for the PSP.

It should be noted that the distance between the blade leading edge and the borescope is confined to ~10 mm due to the geometric restrictions. The vortex shedding from the borescope may affect the film coolant distribution on the leading edge region. However, the response time of current PSP is about 0.3 second to the pressure variation. During 0.3 second, the film cooling blade travels 12–15 revolutions. So, the information from the PSP represents the averaged value and the effect of the wake from the borescope, which is present only at a particular position, is negligible.

2.4. Experimental procedure

For each set of image, 200 pictures were acquired and averaged to calculate the averaged intensity at each pixel. During tests, it was ensured that the temperature of the mainstream air, coolant and test section as well as the rotational speed, torque on the dynamometer and laser output power were in steady state conditions. As the image size obtained from the borescope was slightly larger than each hole, the borescope was traversed along the radial and circumferential to cover the entire leading edge surface. The film cooling holes were used as position markers to align and assemble the pictures together. Reference images were taken at 0-rpm, immediately after performing tests under rotating conditions. Simple MATLAB and FORTRAN programs were used to convert the intensity information into the film cooling effectiveness data.

PSP is sensitive to temperature and hence, the uniformity of the temperature was considered. In general, the mainstream flow may have a temperature variation in radial direction. However, the mainstream flow is highly turbulent and the film cooling flow interrupts with the mainstream flow to yield further mixing. Thus, the temperature variation should be less than a degree. In addition, the blade is made of aluminum. Due to its high thermal conductivity, the temperature variation of a few degrees can be absorbed. So, the error due to the non-uniform temperature distribution would be minimal.

3. Film cooling effectiveness measurement

3.1. PSP measurement theory

As mentioned above, PSP is based on the mass transfer analogy and, thus, eliminates the effects of the heat conduction. Under rotating conditions, this technique can avoid the difficulties incurred in instrumenting the surface with heaters and thermocouples. Thus, PSP technique was adapted in this study.

PSP is a photo-luminescence material that changes emitting light intensity inversely proportional to the surrounding partial pressure of oxygen. By comparing the intensity difference between with and without flow cases, we can obtain the oxygen partial pressure distribution from the following equation:

$$\frac{I_{\text{ref}} - I_{\text{blk}}}{I_{\text{air}} - I_{\text{blk}}} = f\left(\frac{(P_{O_2})_{\text{air}}}{(P_{O_2})_{\text{ref}}}\right) \tag{1}$$

Three kinds of images are needed for data reduction: reference image, air image, and black image. The reference image (I_{ref}) is taken without any mainstream flow but with the coated surface illuminated. The pressure on the test surface $(P_{O_2})_{\text{ref}}$ is constant because there is no flow. The air image (I_{air}) is taken with the mainstream, coolant flows and illuminations. Note that air is used for both mainstream and coolant. The black image (I_{blk}) is taken without any flow or illumination in order to eliminate camera noise. If the function f is available after a proper calibration process (discussed in the following section), the only unknown variable $(P_{O_2})_{\text{air}}$ can be calculated. Most common applica-

tions of PSP are for static pressure measurements. Because the concentration of oxygen is constant ($P_{O_2} = 0.21P$) in the air, the oxygen partial pressure can be converted into the static pressure directly:

$$\frac{(P_{O_2})_{air}}{(P_{O_2})_{ref}} = \frac{(0.21 \times P)_{air}}{(0.21 \times P)_{ref}} = \frac{P_{air}}{P_{ref}} \quad (2)$$

The film cooling effectiveness can be measured using PSP technique by replacing the coolant gas as nitrogen instead of air. In this case, the oxygen (air) as the coolant is replaced with nitrogen which generates lower oxygen partial pressure distribution $(P_{O_2})_{mix}$ on the surface. It can be obtained from the following equation by taking another image: mixture image (I_{mix}). It is taken with the mainstream, coolant flow (nitrogen) and with the surface illuminated

$$\frac{I_{ref} - I_{blk}}{I_{mix} - I_{blk}} = f\left(\frac{(P_{O_2})_{mix}}{(P_{O_2})_{ref}}\right) \quad (3)$$

If the pressure field or molecular weight is assumed to be same between the air and nitrogen injection cases, we can measure the film cooling effectiveness from the difference of the oxygen partial pressure distribution. Note that the film cooling effectiveness can be expressed by a ratio of oxygen concentrations in terms of mass transfer and can be re-written in terms of oxygen partial pressure.

$$\eta = \frac{C_{mix} - C_{air}}{C_c - C_{air}} = \frac{C_{air} - C_{mix}}{C_{air}} = \frac{(P_{O_2})_{air} - (P_{O_2})_{mix}}{(P_{O_2})_{air}} \quad (4)$$

C_{air}, C_{mix}, and C_c are the oxygen concentrations of mainstream air, local mixed gas on the test surface, and coolant gas, respectively.

3.2. Uncertainty calculations

Uncertainty calculations were performed based on a confidence level of 95% and are based on the uncertainty analysis method of Coleman and Steele [32]. The uncertainty for effectiveness is estimated to be 7%, which arises due to an uncertainty of about 5% in the partial pressures of oxygen. This uncertainty is contributed by uncertainties in calibration (4%) and image capture (1%). Also, the level of the shot noise was estimated to be 0.4% [33]. Uncertainty for the blowing ratios is estimated to be 4%. However, the edge of each view window has greater error due to image distortion.

4. Film cooling effectiveness measurement and results

4.1. Calibration of PSP

Calibration for the PSP was conducted inside a vacuum chamber with same optical components and settings. Fig. 8 shows the schematic of the calibration setup. Heated air was circulated until the temperatures of the test sample and the calibration chamber were at steady state at the desired temperature. After that, the inlet of the air flow was blocked and the inside pressure was controlled using a vacuum pump from 0 atm to 1.0 atm. The intensity from the PSP coated test plate was recorded at different pressures. To validate the potential influence of the convex leading edge shape or off-axis lighting/viewing, calibration was conducted on a pipe, whose radius is similar to the curvature of the blade leading edge surface. The calibration result shows that the off-axis lighting/viewing did not affect the result up to ±50°. The view windows of the present experiment results are within the range. Fig. 9 shows the calibration curve of intensity ratio vs. pressure ratio, which is found to be linear except at the high vacuum conditions.

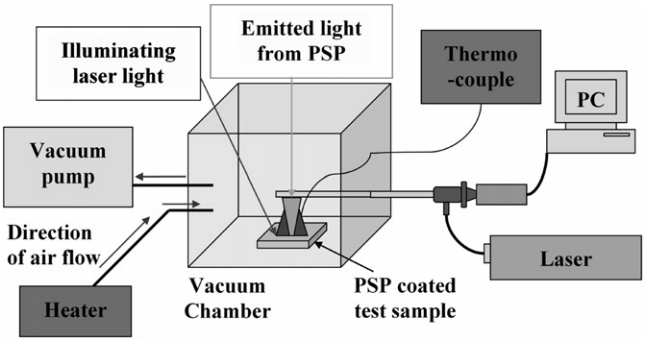

Fig. 8. Schematic drawing of the calibration setup.

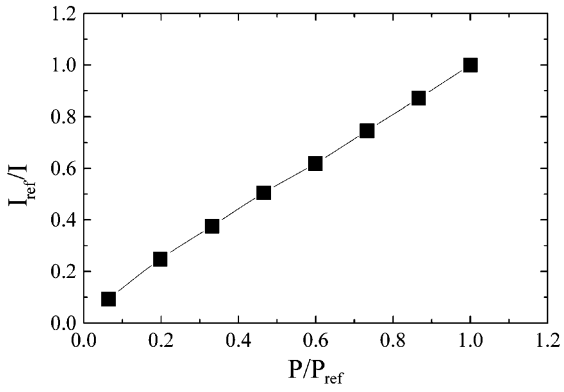

Fig. 9. Calibration curve of the PSP.

4.2. Effects of the rotational speed

Detailed film cooling effectiveness distributions are presented in Figs. 10–12 for each blowing ratio and rotational speed. Inclined lines in each contour represent the approximate stagnation line location relative to the stagnation line location at design condition. Generally speaking, the directions of coolant path lines from the center film cooling row were shifted from the suction side direction to the pressure side direction as the rotational speed increases. At 2400 rpm, the coolant path lines are deflected to the suction side of the rotating blade. At this off-design condition, the mainstream flow approaches the blade at a positive

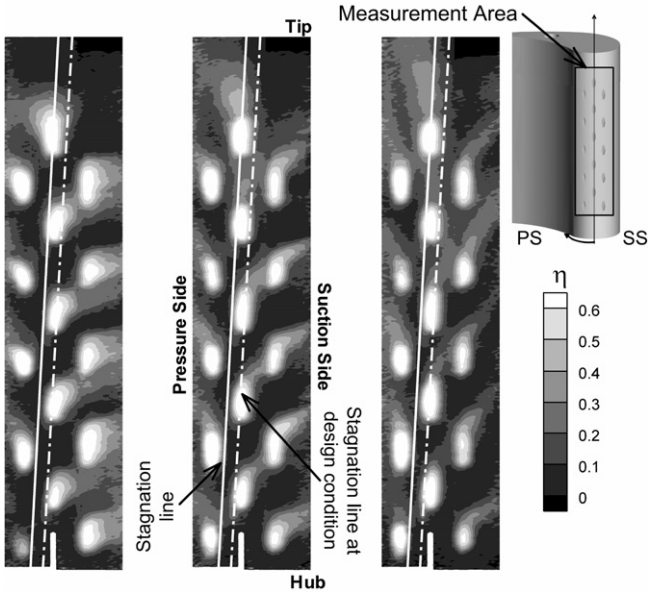

Fig. 10. Film cooling effectiveness distribution at 2400 rpm: (a) $M = 0.5$, (b) $M = 1.0$ and (c) $M = 2.0$.

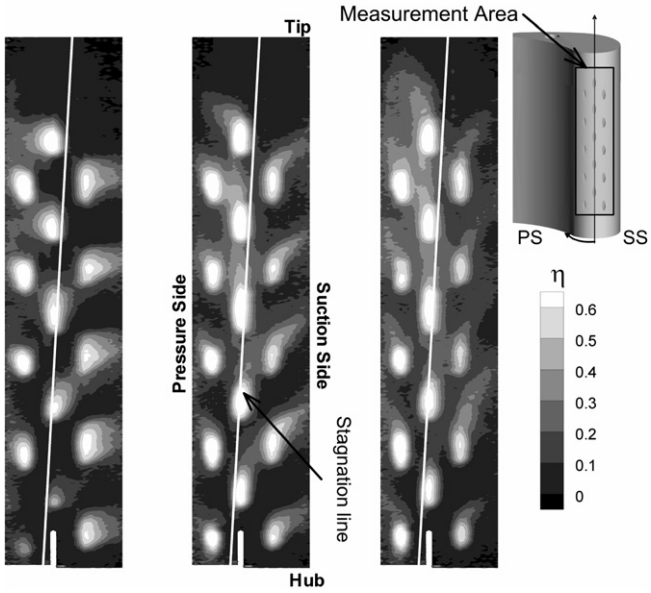

Fig. 11. Film cooling effectiveness distribution at 2550 rpm: (a) $M = 0.5$, (b) $M = 1.0$ and (c) $M = 2.0$.

incidence angle and causing the stagnation line to shift to the pressure side. On the other hand, the mainstream has a negative incidence angle for 3000 rpm, and the stagnation line is shifted to the suction side. These phenomena have been graphically explained in Fig. 13. Because the direction of the flow near the blade surface is opposite to each other at these two off-design conditions, the direction of the coolant flow also changes. At 2550 rpm case (design point), the coolant path lines from the holes near the hub are deflected

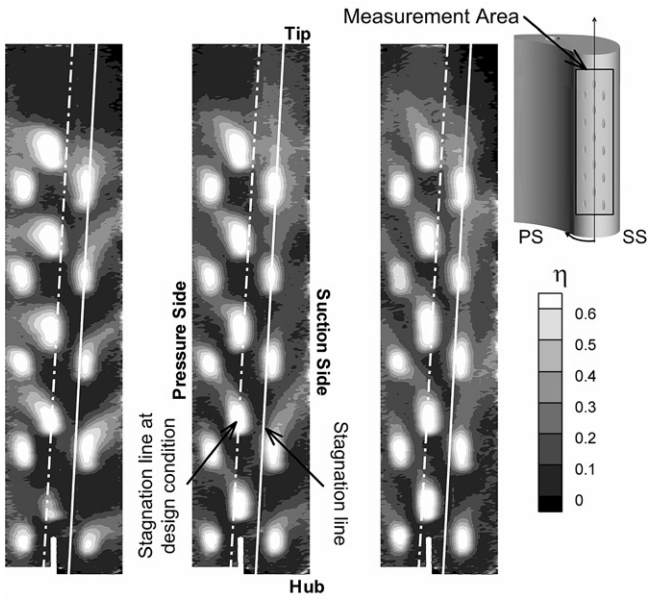

Fig. 12. Film cooling effectiveness distribution at 3000 rpm: (a) $M = 0.5$, (b) $M = 1.0$ and (c) $M = 2.0$.

to the suction side and the holes near the tip are deflected to the pressure side. Note that a 2-dimensional blade design was used in this study. The relative inlet angle to the blade is a function of the blade height, because the circumferential velocity increases with blade height. As a result, the stagnation line is slightly inclined. For the coolant flows from the other rows, the directions of the flow were consistent although the deflection amount was affected by the rotational speed.

The coolant traces from the suction side row flow to the suction side at 2400 rpm and get closer to the span-wise direction as the rotational speed increases. Regarding the degree of the deflection, there is a larger difference between the 2550 rpm and 3000 rpm cases compared to the difference between the 2400 rpm and 2550 rpm cases. For 3000 rpm, there is a larger difference in the rotational speed from the design point as compared to 2400 rpm. As a result, the absolute value of the incidence angle of the mainstream and its effect on the coolant flow direction is larger for the 3000 rpm case compared to the 2400 rpm case.

On the pressure side, however, the difference of the coolant flow angle is minimal. The difference in the rotational speed changes the incidence angle and the stagnation location. This changes the direction of the mainstream flow near the center row and suction side row. Near the pressure side row, however, due to smaller rotational speed differential between 2400 rpm and 2550 rpm (design point), the shift of the stagnation line is not large enough to change the direction of the coolant flow. It seems the stagnation line is located between the pressure side and center rows at 2400 rpm. As the rotational speed increase, the stagnation line relocates near the center row and suction side row at 2550 rpm and 3000 rpm cases respectively.

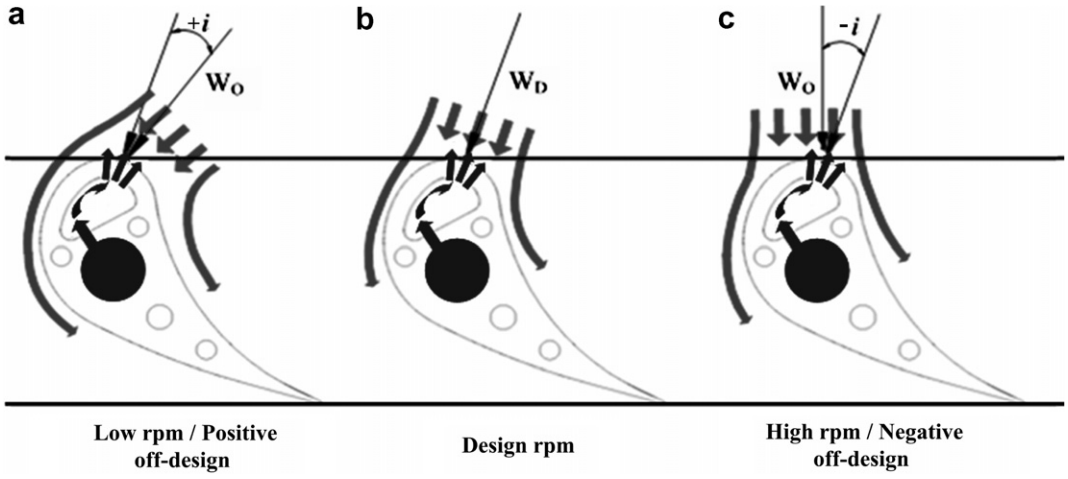

Fig. 13. Flow path inside and outside the blade for (a) positive off-design, (b) design, and (c) negative off-design conditions.

4.3. Effect of averaged blowing ratio

The averaged blowing ratio was controlled to be 0.5, 1.0, and 2.0 for each rotational speed. As mentioned above, the direction of the coolant flow is affected by the blowing ratio. At $M = 0.5$, coolant flows have smaller momentum and the mainstream flow dominates the coolant flow path direction. As the blowing ratio increases, the momentum of the coolant flow also increases and is comparable to the momentum of the mainstream flow. As a result, the coolant flow traces appear to head towards the blade tip, which is the direction of the coolant ejection. It seems there is more mixing between the mainstream and coolant flow at higher blowing ratio due to the increased interaction. So, the coolant traces downstream of each film cooling hole decay faster as compared to the lower blowing ratio case. On the other hand, increased mixing provides slightly more uniform film distribution. Lift-off phenomena also contribute to the weaker coolant traces at higher blowing ratio.

4.4. Effect of local blowing ratio

The coolant injection is driven by the pressure difference between the blade inner cavity and the blade outer surface. Because the pressure inside the cavity should be same for all the film cooling holes, the local blowing ratio is directly determined by the surface static pressure, which is affected by the location of the stagnation line. Especially, in the case of $M = 0.5$, the momentum of the coolant flow is much smaller than the mainstream and the reduction of the local blowing ratio is quite significant if the stagnation line locates on the hole. At 2400 rpm, the stagnation line is located between the pressure and center row and the local blowing ratio is quite uniform except for the bottom hole on the pressure side. For 2550 rpm, the stagnation line is located on the center row. As a result, the strength of the coolant traces from the center row for $M = 0.5$ case is weaker compared to other rotational speeds. However, as the blowing ratio increase, it seems the stagnation location does not suppress the coolant injection much because as the coolant jet has a higher momentum than mainstream. On the suction side row for $M = 1.0$ and 2.0 cases, low film effectiveness level can be observed, possibly due to the lift-off of the coolant. For 3000 rpm case, the stagnation line shifts toward the suction side and is located near the suction side row, suppressing the coolant injection. Thus, the film effectiveness level near the suction side row is lower for $M = 0.5$ case. At higher blowing ratios of 1.0 and 2.0, the momentum of coolant gas is strong enough to overcome the mainstream flow and the effectiveness level on the suction side row is comparable to those on the other rows.

4.5. Span-wise averaged film cooling effectiveness

Span-wise averaged effectiveness distributions are shown in Fig. 14. Generally speaking, $M = 1.0$ and 2.0 cases shows similar profile while the $M = 0.5$ case shows different behavior in terms of effectiveness level and decaying rate. Two thousand and four hundred rpm case is shown in Fig. 14(a). At $M = 0.5$ case, suction side shows the highest effectiveness level and slow decaying rate. In this case, the coolant flows from the center row are deflected to the suction side and fill the spaces between the suction side film cooling holes. So, more area on the suction side is protected by the coolant film, which explains the higher level on this side. On the other hand, the pressure side area does not have much benefit from the center row. At $M = 1.0$ and 2.0 cases, the deflections of the coolant traces are less and more coolant gas heads in the span-wise direction. So, the shape of the span-wise averaged effectiveness profiles are sharper as compared to those for the $M = 0.5$ case. The averaged effectiveness level also increases as compared to the $M = 0.5$ case on the center and pressure row area due to the smaller deflection of the coolant gas. For the suction side area, however, the averaged effectiveness level of $M = 1.0$ and 2.0 is smaller than the $M = 0.5$ case. One of the reasons is the reduced benefit from the center row as

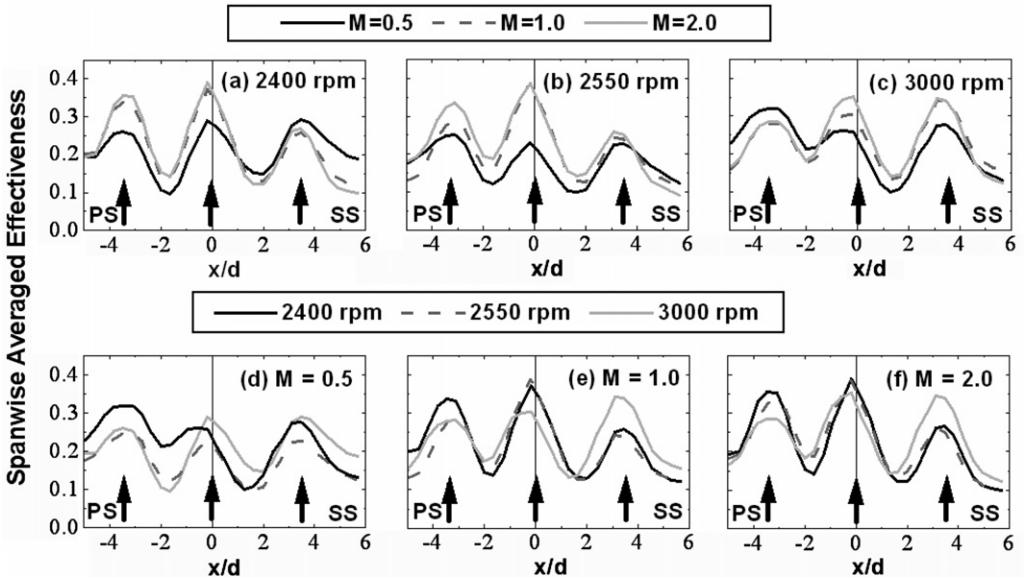

Fig. 14. Span-wise averaged film cooling effectiveness.

explained in the previous section. In addition, the non-uniform local blowing distribution increases the local blowing ratio on the suction side. Thus, the coolant from the suction side row will penetrate into the mainstream, or lift-off from the surface. This phenomenon explains the lower effectiveness level and faster decay rate near the suction side row.

At 2550 rpm, the stagnation line located near the center row suppresses the coolant injection for $M = 0.5$ case. At $M = 1.0$ and 2.0, however, the effectiveness on the center row is very high as compared to the other rows. It seems that the coolant flow on the center row has enough momentum to reach to the surface, but not enough to penetrate into the mainstream. Thus, they have more chance to stay on the blade surface and give better protection. On the pressure and suction side rows, the effectiveness is lower, which may due to the lift-off. However, both side rows have benefit from the center row and the coolant is distributed uniformly. So, their averaged effectiveness level is higher than the $M = 0.5$ case.

On the pressure side at 3000 rpm, $M = 0.5$ case shows the highest film effectiveness level. As the stagnation line is located between the center and suction side row, the coolant traces from the center row are deflected to the pressure side and contribute to the higher film effectiveness level. Near the center row of $M = 0.5$ case, the deflection of the coolant traces are quite significant. Thus, the area between the center-row holes is not covered by the coolant film and shows lowest film effectiveness level among the three blowing ratio cases. On the suction side row of $M = 0.5$, the area between the holes are still not much protected by the coolant film. However, the deflection of the coolant traces are smaller and show moderate film effectiveness level compared to the center and pressure side row regions. As the blowing ratio increases, the coolant traces show a larger tendency to flow in the span-wise direction. As a result, the film effectiveness level on the suction side decreases and those on the other rows increases.

5. Conclusions

Detailed film cooling effectiveness distributions were measured on the leading edge region of a rotating blade with three rows of radial-angle holes by using the PSP measurement technique. The major findings of this study are as follows:

1. The rotational speed is the most critical parameter in determining the film cooling effectiveness distributions. It changes the mainstream incidence angle to the leading edge and affects the film cooling flow path direction.
2. The film cooling flow path of the leading edge center row heads to the suction side, span-wise, and pressure side direction at 2400, 2550, and 3000 rpm, respectively.
3. The effects of the rotational speed on the pressure and suction side row film cooling are not as strong as that on the leading edge center row film cooling.
4. As the blowing ratio increases, the distribution of the leading edge region film cooling is more uniform and the averaged film cooling effectiveness level slightly increases (Table 2).

Table 2
Averaged film effectiveness on the interested area

Item	$M = 0.5$	$M = 1.0$	$M = 2.0$
2400 rpm	0.211	0.222	0.223
2550 rpm	0.176	0.210	0.225
3000 rpm	0.221	0.232	0.238

5. The location of the stagnation line affects the local blowing ratio. The coolant injection near the stagnation line was suppressed, especially for the lower blowing ratio case, $M = 0.5$.

Acknowledgements

This work was prepared with the support of Solar Turbines, Inc. The authors appreciate their help and support. The authors also thank to our co-worker, Burak Ozturk for helpful discussions and comments.

References

[1] J.C. Han, S. Dutta, S.V. Ekkad, Gas Turbine Heat Transfer and Cooling Technology, Taylor & Francis, New York, 2000.
[2] N.V. Nirmalan, L.D. Hylton, An experimental study of turbine vane heat transfer with leading edge and downstream film cooling, ASME J. Turbomach. 112 (1990) 477–487.
[3] N. Abuaf, R. Bunker, C.P. Lee, Heat transfer and film cooling effectiveness in a linear airfoil cascade, ASME J. Turbomach. 119 (1997) 302–309.
[4] M.W. Cruse, U.M. Yuki, D.G. Bogard, Investigation of various parametric influences on leading edge film cooling, ASME Paper 97-GT-296, 1997.
[5] S.V. Ekkad, A.B. Mehendale, J.C. Han, C.P. Lee, Combined effect of grid turbulence and unsteady wake on film effectiveness and heat transfer coefficient of a gas turbine blade with air and CO_2 Film Injection, ASME J. Turbomach. 119 (1997) 594–600.
[6] J.M. Cutbirth, D.G. Bogard, Effects of coolant density ratio on film cooling performance on a vane, in: Proceedings of ASME Turbo Expo 2003, Atlanta, Georgia, GT2003-38582, June, 2003.
[7] D.W. Luckey, D.K. Winstanley, G.J. Hames, M.R. L'Ecuyer, Stagnation region gas film cooling for turbine blade leading-edge applications, AIAA J. Aircraft 14 (1977) 494–501.
[8] W.J. Mick, R.E. Mayle, Stagnation film cooling and heat transfer including its effect within the hole pattern, ASME J. Turbomach. 110 (1988) 66–72.
[9] J. Karni, R.J. Goldstein, Surface injection effect on mass transfer from a cylinder in crossflow: a simulation of film cooling in the leading edge region of a turbine blade, ASME J. Turbomach. 112 (1990) 418–427.
[10] A.B. Mehendale, J.C. Han, S. Ou, Influence of high mainstream turbulence on leading edge heat transfer, ASME J. Heat Transfer 113 (1991) 843–850.
[11] A.B. Mehendale, J.C. Han, Influence of high mainstream turbulence on leading edge film cooling heat transfer, ASME J. Turbomach. 114 (1992) 707–715.
[12] S. Ou, A.B. Mehendale, J.C. Han, Influence of high mainstream turbulence on leading edge film cooling heat transfer: effect of film hole row location, ASME J. Turbomach. 114 (1992) 716–723.
[13] A.B. Mehendale, J.C. Han, Reynolds number effect on leading edge film effectiveness and heat transfer coefficient, Int. J. Heat Mass Transfer 36 (15) (1993) 3723–3730.
[14] M. Salcudean, I. Gartshore, K. Zhang, Y. Barnea, Leading edge film cooling of a turbine blade model through single and double row injection: effects of coolant density, ASME Paper 94-GT-2, 1994.
[15] K. Funazaki, M. Yokota, K. Yamawaki, The effect of periodic wake passing on film effectiveness of discrete holes around the leading edge of a blunt body, ASME J. Turbomach. 119 (1997) 292–301.
[16] S.V. Ekkad, J.C. Han, H. Du, Detailed film cooling measurements on a cylindrical leading edge model: effect of free-stream turbulence and coolant density, ASME J. Turbomach. 120 (1998) 799–807.
[17] S. Ou, R.B. Rivir, Leading edge film cooling heat transfer with high free stream turbulence using a transient liquid crystal image method, Int. J. Heat Fluid Flow 22 (2001) 614–623.
[18] H. Reiss, A. Bölcs, Experimental study of showerheat cooling on a cylinder comparing several configurations using cylindrical and shaped holes, J. Turbomach. 122 (2000) 161–169.
[19] Y.J. Kim, S.M. Kim, Influence of shaped injection holes on turbine blade leading edge film cooling, Int. J. Heat Mass Transfer 47 (2004) 245–256.
[20] R.P. Dring, M.F. Blair, H.D. Hoslyn, An experimental investigation of film cooling on a turbine rotor blade, ASME J. Eng. Power 102 (1980) 81–87.
[21] K. Takeishi, M. Matsuura, S. Aoki, T. Sato, An experimental study of heat transfer and film cooling on low aspect ratio turbine nozzles, ASME J. Turbomach. 112 (1990) 488–496.
[22] R.S. Abhari, A.H. Epstein, An experimental study of film cooling in a rotating transonic turbine, ASME J. Turbomach. 116 (1994) 63–70.
[23] L.J. Zhang, M. Fox, Flat plate film cooling measurement using PSP and gas chromatography techniques, in: Proceedings of the Fifth ASME/JSME Joint Thermal Engineering Conference, San Diego, CA., 1999.
[24] L.J. Zhang, M. Baltz, R. Pudupatty, M. Fox, M., Turbine nozzle film cooling study using the pressure sensitive paint (PSP) technique, ASME Paper No. 99-GT-196, 1999.
[25] L.J. Zhang, R.S. Jaiswal, Turbine nozzle endwall film cooling study using pressure-sensitive paint, ASME J. Turbomach. 123 (2001) 730–738.
[26] J. Ahn, S. Mhetras, J.C. Han, Film-cooling effectiveness on a gas turbine blade tip using pressure sensitive paint, in: Proceedings of ASME Turbo Expo 2004, GT-2004-53249, 2004.
[27] S. Mhetras, H. Yang, Z. Gao, J.C. Han, Film-cooling effectiveness on squealer rim walls and squealer cavity floor of a gas turbine blade tip using pressure sensitive paint, in: Proceedings of ASME Turbo Expo 2005, GT 2005-68387, 2005.
[28] L.M. Wright, Z. Gao, T.A. Varvel, J.C. Han, Assessment of steady state PSP, TSP, and IR measurement techniques for flat plate film cooling, in: Proceedings of 2005 ASME Summer Heat Transfer Conference, HT 2005-72363, 2005.
[29] Z. Gao, L.M. Wright, J.C. Han, Assessment of steady PSP and transient IR measurement techniques for leading edge film cooling, in: Proceedings of 2005 ASME IMECE Congress and Exposition, IMECE2005-80146, 2005.
[30] M.T. Schobeiri, J.L. Gillaranz, E.S. Johansen, Aerodynamic and performance studies of a three stage high pressure research turbine with 3-D blades, design points and off-design experimental investigations, in: Proceedings of ASME Turbo Expo 2000, 2000-GT-484, 2000.
[31] M.T. Schobeiri, A. Suryanarayanan, C. Jermann, T. Neuenschwander, A comparative aerodynamic and performance study of a three-stage high pressure turbine with 3-D bowed blades and cylindrical blades, ASME Paper GT2004-53650, 2004.
[32] H.W. Coleman, W.G. Steele, Experimentation and Uncertainty Analysis for Engineers, John Wiley & Sons, New York, 1989.
[33] T. Liu, M. Guille, J.P. Sullivan, Accuracy of pressure sensitive paint, AIAA J. 39 (n1) (2001) 103–112.